Monitoring Ion Therapy with a Compton Camera: Simulation Studies of the Clinical Feasibility

J.-L. Ley[1], C. Abellan[2], J.-P. Cachemiche[2], M. Dahoumane[1], D. Dauvergne[1], N. Freud[3], B. Joly[4], J. Krimmer[1], J. M. Létang[3], L. Lestand[4], H. Mathez[1], G. Montarou[4], M. Pinto[1], M-.H. Richard[1], E. Testa[1] and Y. Zoccarato[1]

[1]Université de Lyon, Université Claude Bernard Lyon 1, CNRS/IN2P3, Institut de Physique Nucléaire de Lyon, 69622 Villeurbanne; MICRHAU pôle de Microélectronique Rhône Auvergne, France
[2] CPPM, Aix-Marseille Université, CNRS/IN2P3, Marseille
[3] Université de Lyon, CREATIS; CNRS UMR5220; Inserm U1044; INSA - Lyon; Université Lyon 1; Centre Léon Bérard, France
[4]Laboratoire de Physique Corpusculaire de Clermont-Ferrand, France

E-mail: `jeanluc.ley@gmail.com`

Abstract. The aim of irradiation monitoring during a treatment in ion therapy is to control in real time the agreement between the delivered dose and the planned treatment. In fact, the discrepancies might come from uncertainties such as the planning accuracy by itself, or by variations due to the positioning or the anatomical changes of the patient. This can lead to ion-range variations of a few millimeters. Several devices are under development over the world to detect secondary radiations, which are correlated to the dose deposited by incident ions [1]. Compton cameras are in particular investigated for their potential high efficiency to detect prompt-gammas [2-5]. The present work aims at discussing the clinical applicability of a Compton camera design by means of Monte Carlo simulations validated against measurements of single and coincidence rates.

1. Introduction

2. Material and methods

2.1. Simulation setup

The simulation consists of the irradiation of a patient by an ion beam and the detection of the secondary particles emitted by mean of the Compton camera prototype. The patient is replaced by a cylindrical PMMA† phantom of 15 centimeters diameter and 20 centimeters length. The Compton camera prototype is composed by a scatterer, an absorber and a scintillating fiber hodoscope. The scatterer is a stack of seven layers of double-sided silicon strip detectors (DSSD) of $90 \times 90 \times 2$ mm^3 with 64 strips on each side. The absorber consists of 96 blocks of streaked BGO† crystals of $38 \times 38 \times 30$ mm^3. The hodoscope is formed by 2×128 square scintillating fibers of 1 mm^2 and 140 mm length of BCF 12. The mechanical structures of the detectors, the scatterer's strips and the hodoscope are not modelled in this study. Moreover, the absorber is modelled by a monoblock of BGO crystal of $380 \times 380 \times 30$ mm^3 equivalent to 100 single blocks. The distance between the camera and the center of the PMMA phantom is set at 20 centimeters in order to fit with a realistic distance to the patient. The distance between each silicon layer is one centimeter and the distance from the last silicon layer to the absorber is 40 centimeters. The distance between the stack of silicon layers and the absorber is a compromise between the camera efficiency and the discrimination by time of flight measurement. The setup is described figure 1.

2.2. Hadronic models used in Geant4

The study is based on the Monte Carlo methods with the Geant4 toolkit, version 9.6 patch 02. Geant4 has been developed by the CERN for the high energy physics experiments. It was shown, that it could be also used in ion therapy studies [Cirrone et al., 2011, Toshito et al., 2010]. However, some improvements remains to do in order to adjust the hadronic models [Dedes et al., 2014] . The interaction processes in the matter are described by means of different models according to the type of particles. A resume of those different models is given table 1. Additionally, the Doppler broadening and the polarization is taking into account.

2.3. Particles of interest

We study the two main particles used in clinic, namely the protons and the carbon ions. The ion range of interest is 15.2 cm in the PMMA target. The energies associated to

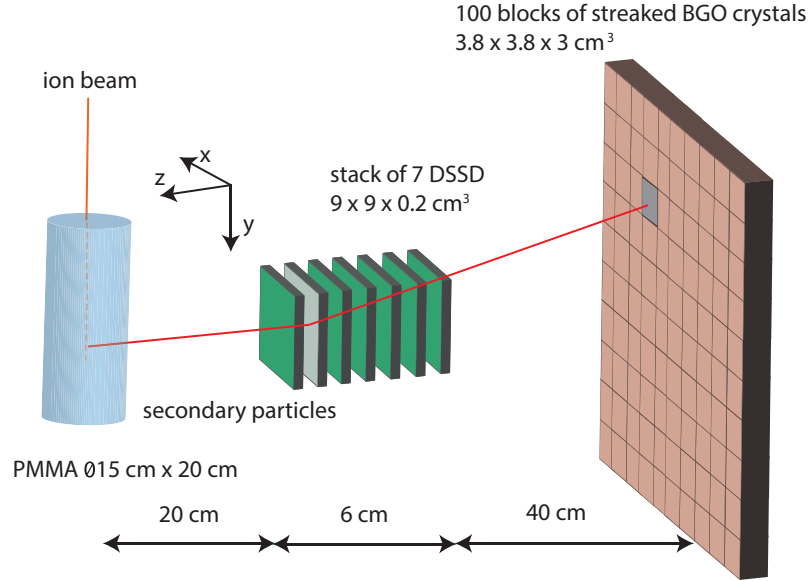† PolyMethylMethAcrylate
† Bismuth Germanate

Figure 1: Modelling of the patient (PMMA cylinder) and the Compton camera prototype. This configuration is used for all the results presented in this paper.

Table 1: Hadronic models used in the simulations Geant4.

Processus	Protons	Ions	Neutrons
Electromagnetic		standard$_{option3}$	
Inelastic	G4BinaryCascade	G4QMDReaction	G4BinaryCascade
		(G4IonsShenCrossSection)	+ G4NeutronHPInelastic ($<$19 MeV)
Elastic	G4LElastic	G4LElastic	G4LElastic + G4NeutronHPElastic ($<$19 MeV)
Fission	/	/	G4LFission + G4NeutronHPFission($<$19 MeV)
Capture	/	/	G4LCapture + G4NeutronHPCapture ($<$19 MeV)
Radioactivedecay	/	G4Radioactivedecay	/

the range is 160 MeV for the protons and 305 MeV/n for the carbon ions. The beam delivered during a real treatment has a gaussian profile at the enter of the patient. The standard deviation for a proton beam is 5 mm at 160 MeV and 3.5 mm for a carbon ion beam at 305 MeV/n. The modelling of the Compton camera does not change with the type of incident particles. The statistic for a spot in pencil beam scanning (PBS) mode for protons is 10^8 particles and 10^5 particles for carbon ions. The beam time structure is applied during the post treatment.

2.4. Data treatment

2.4.1. Detector's resolutions

The Monte Carlo simulation parameters are as close to reality as possible in order to get relevant results. The detector resolutions play an important role in the Compton

camera performances. The absorber's spatial resolution influences the position of the apex of the Compton cone and influences its axis orientation. The energy resolution has effect on the Compton cone aperture angle and the timing resolution impacts the coincidence windows between the absorber and the scatterer. The hodoscope is not included in the simulation but its timing resolution is taking into account for the time of flight discrimination. The detector resolutions are modelled in relation to the resolutions measured or estimated for each detector. The spatial resolution, the energy resolution and the timing resolution are presented in the table 2.

Table 2: Realistic resolutions applied during the simulations.

Résolution (FWHM) à 1 MeV	Scatterer Si	Absorber BGO	Hodoscope
spatial [mm]	0.9	5	/
energy [%]	2.3	17	/
timing [ns]	15	3	1

2.4.2. Modelling of the ion beam structure

The beam time structure should have a direct impact on the Compton camera capacities to detect a particle in coincidence between the scatterer and the absorber. Two beam time structures have been modelled: one of IBA cyclotron C230 for protons (used in 16 clinical centers worldwide) and one of synchrotron installed at the Heidelberg Ion Therapy Center (HIT) in Germany for carbon ions. Depending the ion energy and the beam intensity, the beam microstructure will change. We are focusing in this study to the microstructure at a specific energy and at the influence of the variation of the intensity. In the case of protons at 160 MeV, the ions are grouped in bunches of 2 ns at a frequency of 106 MHz (9.42 ns) [F Roellinghoff, 2014]. The clinical beam intensity is 3.2 nA which corresponds to about 200 protons per bunch. Concerning the carbon ion beam at 305 MeV/u, the estimated microstructure is a bunch of 30 ns at a frequency of 5.9 MHz (170 ns). The clinical beam intensity for carbon ions is 5×10^7 ions/s which corresponds to about 9 ions per bunch This beam structure is extrapolated from measurements done by our team in 2013 at HIT. The time beam structure was measured for 200 MeV/u and 400 MeV/u carbon ions beam with a two scintillating fibers hodoscope and the spill signal given by the accelerator. The figure 2 shows the beam structure for carbon ions at 400 MeV/u. The pulses have a spill period of 150.2 ns and a bunch is 21.5 ns. A dedicated measure should be done for the energy of interest for this study (305 MeV/u).

Moreover, the measurements have showed that the spill phase change during the extraction which involves that the HF signal from the synchrotron can not be used to locate the pulses. The use of the hodoscope seems required.

In term of the coincidence between the scatterer and the absorber, we allow a time window of 40 ns around an absorber event. It means that for an event detected in
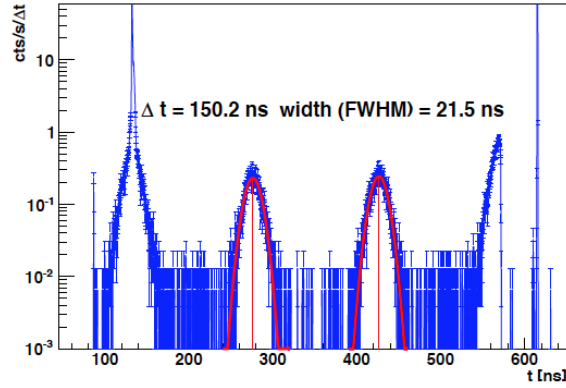
Figure 2: Time structure measured from a carbon ion beam at 400 MeV/u delivered at HIT. The pulses have an extraction period of 150.2 ns and the bunches are 21.5 ns FWHM. The measure was done with a two scintillating fibers hodoscope.

the absorber, it will be flagged as a coincidence if an event (corresponding to a deposit energy) in one the scatterer layers is detected in a window of -20 ns and + 20 ns around the absorber event. This coincidence windows is defined regarding of the silicon timing resolution which is 15 ns at the full width at half maximum.

Table 3: Beam structure applied to the simulation datas.

		Protons	Carbon ions
Clinical characteristics	Facility	IBA Cyclotron C230	Synchrotron at HIT
	Clinical intensity	2×10^{10} p/s	5×10^7 ions/s
	Energy	160 MeV	305 MeV/u
Beam structure	Bunch time [ns]	3.2	30
	Period [ns]	9.4	170
	Particles/bunch	217	9
Detectors	Coincidence window [ns]	40	40
	Timing resolution [ns]	Si: 15 and BGO: 3	

2.4.3. Coincidence

A coincidence is defined as one energy deposit in the scatterer and one energy deposit in the absorber in a coincidence time windows given. The Compton camera is based on a double interaction inside the scatterer and the absorber. However, a number of events will be considered as background: quasi-simultaneous interaction from
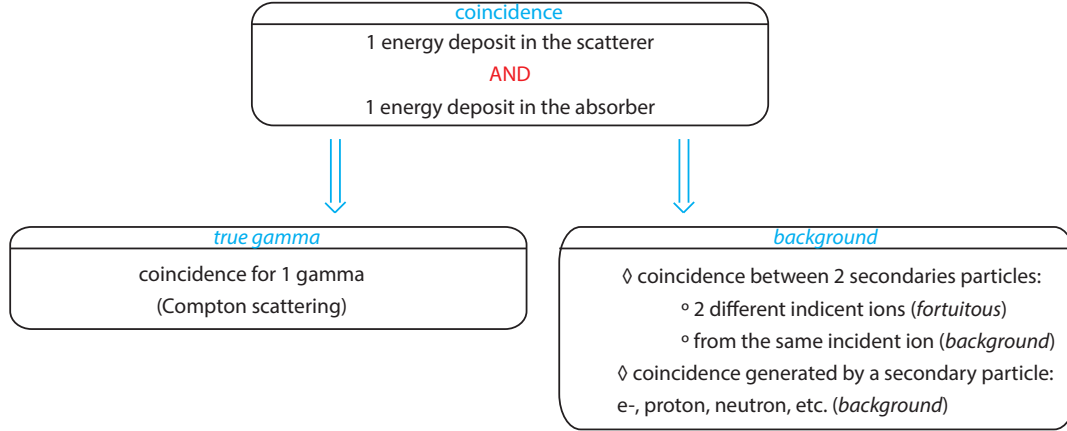

Figure 3: Diagramme reprenant la définition d'une coïncidence et des distinctions faites pour classifier les différents cas de figure.

As mentioned before, a coincidence is defined as an energy deposit in one silicon layer of the scatterer stack and an energy deposit in the BGO absorber. The deposit energies in the detectors can come from the same particle or can come from two different one. In the case of distinct radiations, if the the two particles are originated from the same incident ion on the target, the coincidence is named true coincidence. Otherwise, if this is not, so the coincidence is named a random coincidence. A more detailed analysis leads to separate the true coincidences in subparts.

- The same secondary particle interacts in the scatterer and the absorber and make a coincidence. The secondary particle can be:
  - A gamma ray.
  - An other type of charged particles: neutron, proton, electron.
- Two different types of secondary particle makes a coincidence: one interacts in the scatterer and the other in the absorber.

As the Compton camera's goal is to detect the gamma's scattering in the scatterer then its full absorption in the absorber, a coincidence corresponding to this definition is named a true gamma coincidence. The other type of coincidences is labeled background.

2.4.4. Time of flight discrimination and energy cuts

Time of flight (TOF) information

The objective is to eliminate the massive or charged particles (proton, electron, neutron) creating a coincidence in the Compton camera thanks to their speed. In fact,

the photons are moving at the light speed when the other particles are moving slower due to their mass. To discriminate the particles with their speed, the time information coming from the hodoscope and the time information coming from the absorber are used. The difference between those informations is named time of flight (equation 1). However, the hodoscope is not modeling in this study. As the Monte Carlo code consists to follow all story individually, the time between the incident particle's creation and the secondary particle detection in the absorber is considered as the time of flight. Moreover, the hodoscope has a timing resolution about one nanosecond at full width at half maximum, so it is taking into account in the TOF estimation.

$$TOF_{theoretical} = t_{absorber} - t_{hodoscope}$$
$$TOF_{simulation} = t_{absorber} + t_{creation} + u_{hodoscope}$$

With $u_{hodoscope}$ the hodoscope resolution modeled by a gaussian with a sigma of $1/2.35$ ns.

The time of flight spectrum resulting from the simulation shows that the coincidences of interest are included in a window between 0 and 6 ns (Fig. X). Therefore, all the coincidences with a TOF higher than 6 ns will be excluded of the results.

Figure 4: Time of flight spectrum obtained by mean of the simulation and for a proton beam.
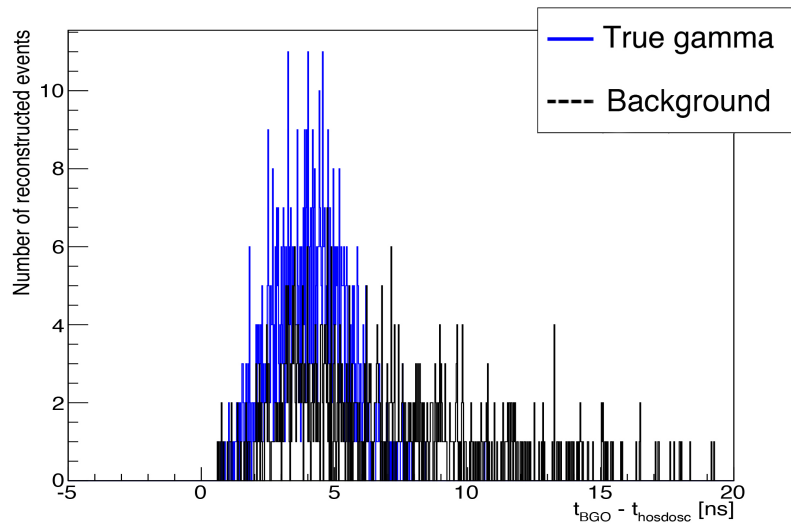
Energy cuts

Energy triggers are also defined for the detectors: 50 keV for the silicon layers and 100 keV for the absorber. An additional energy cut is practiced to the total energy absorbed in the camera and it is set at one MeV. In fact, the main gamma rays of interest have an energy upper at one MeV.

2.5. Reconstruction algorithm

A simple method is used to reconstructed the emission position of the events detect in coincidence: the reconstruction line-cone. Thanks to the energies deposited in the detectors and the interaction positions, a cone is calculated which contains the event emission point. The energies enable to calculate the aperture of the Compton's cone by way of the following equation:

$$cos(\theta_{Compton}) = 1 - m_e c^2 \left(\frac{1}{E_{absorber}} - \frac{1}{E_{initial}} \right) \tag{1}$$

With $E_{initial} = E_{absorber} + E_{silicon}$
$E_{absorber}$ the energy deposited in the absorber and $E_{silicon}$ the energy deposited in the scatterer.

We assume that the initial energy of the gamma ray is fully absorbed in the absorber. This hypothesis combined to the detector energy resolutions lead to a potentiel uncertainty on the cone aperture. The interaction position in the scatter gives the cone apex and the position in the absorber gives the cone axis. The intersection of all the reconstructed cones gives the emission source point. In order to simplify the reconstruction and limit the possibilities, the beam direction is used to obtain just two solutions: the beam direction intersects the cone in two points. Only one of those solutions is the good one and the other will give a wrong information. As the original position is unknown when the gamma ray is detected in coincidence, the results presented in the next section take into account the two solutions.
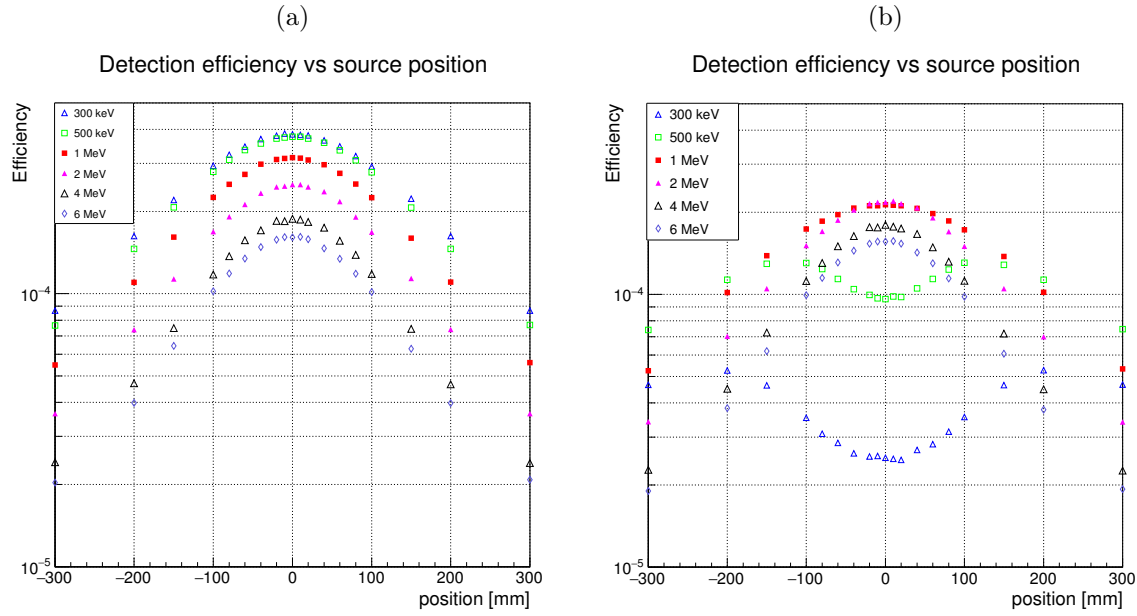
2.6. Precision estimation

Figure 5: Line cone - MLEM.

(a)

(b)

(c)

(d)

(e)

(f)

(g)

(h)
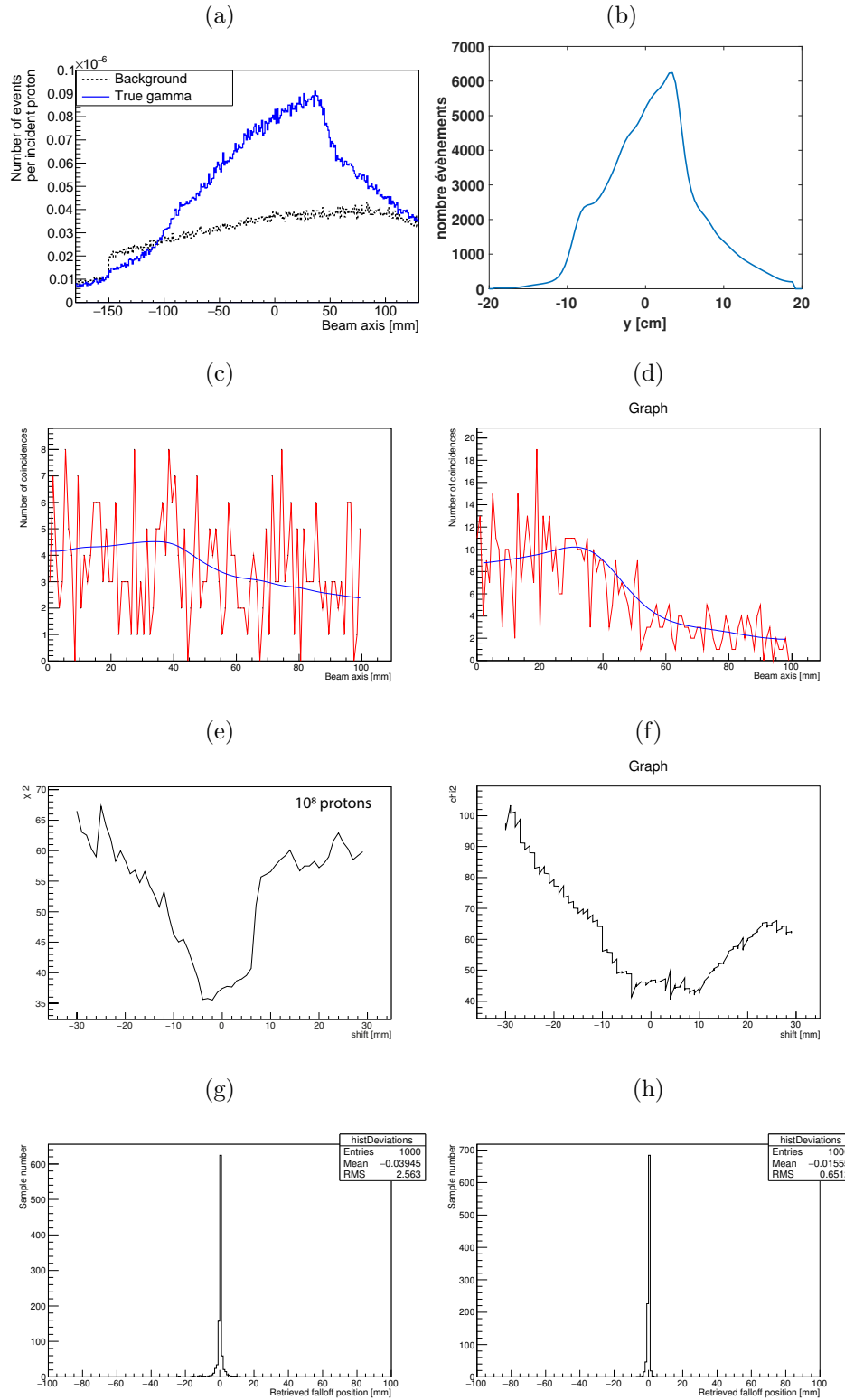
## 3. Results

3.1. CC efficiency

Figure 6: Detection efficiency function of the Compton Camera position.

(a) (b)

J'assigne à chaque particule interagissant dans le diffuseur et l'absorbeur un numéro de paquet auquel elle est théoriquement rattachée au vu de la structure en temps choisie et de l'intensité du faisceau. The modification of the beam intensity will change the number of particles included in a bunch. For instance, at the clinical intensity in proton, there is in average 217 protons in a bunch.

The beam intensity plays an important role for the Compton camera concerning its capability to distinct events in coincidence. In the simulation, the beam intensity is modeled by an average number of particles per bunch. The exact number of particles in each bunch is given by a random draw in a Poisson distribution, where the mean value is the beam intensity chosen. The range of intensities was chosen in order to cover almost all the possibilities: from a very low beam intensity to the clinical beam intensity. Therefore, for proton and carbon ion, the lowest beam intensity is set to 0.001 particles per bunch in average and for protons goes up to 217 protons per bunch when in case of carbon ion, it goes up to 70 particles per bunch. The coincidence yields are scaled per ion incidents and the beam intensity per average ions per bunch. The true coincidences represent a coincidence in the camera by the same gamma ray. The background corresponds to all the other coincidence types.

Figure 7: Coincidences yield for protons (a) and carbon ions (b) in function of the beam intensity. The intensity is given for a number of incident particles per bunch. The distinction between the filled markers and the empty ones are that the time of flight discrimination is applied in the case of empty markers.

(a) (b)
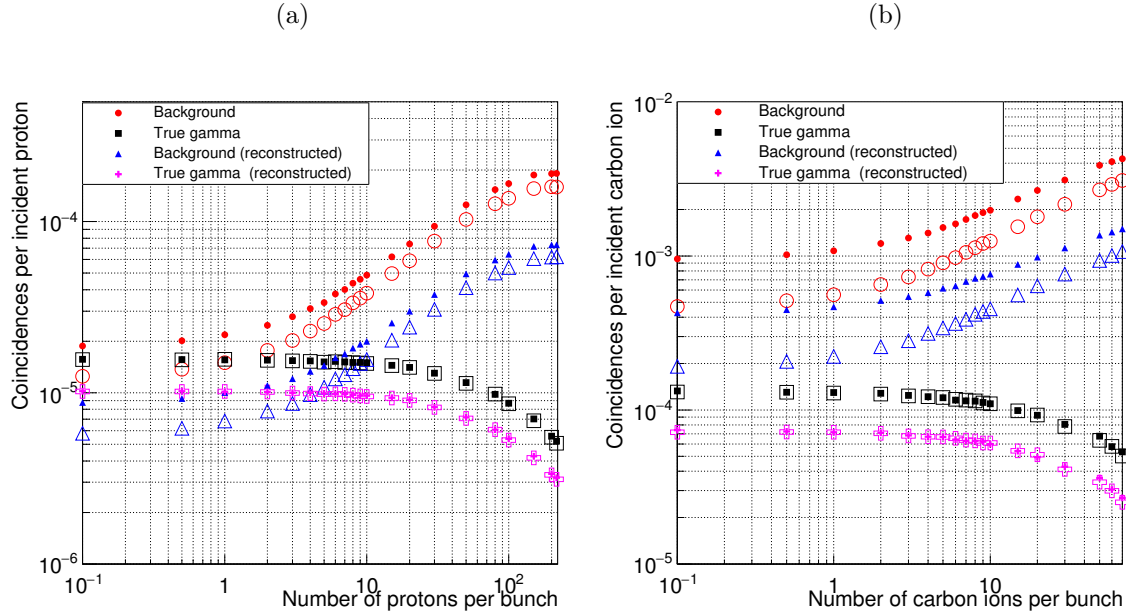
At the clinical beam intensity, the high background level is mainly due to the random coincidences. In fact, the probability to detect two radiations coming from two different incident particles increases with the number of incident particles per bunch. An other issue is the single rate of events detected by each detectors at those high intensities. For instance, at the clinic beam intensity in proton therapy, the single rate on the absorber is around 300 MHz and on the first silicon layer it is around 20 MHz. The current electronic front end and acquisition system are not able to treat this amount of data coming from all the detectors. As a result, it appears that it is impossible to use the Compton camera at a clinical beam intensity for the treatment monitoring in ion therapy.

Nevertheless, if the intensity decreases enough to avoid almost all the random coincidences, the monitoring seems more feasible. In addition, it can be suppose that the time of flight discrimination will improve the signal to background ratio at low intensities by suppress the coincidences induced by charged particles. Indeed, the charged particles are slower than gamma rays which move at the light speed.

Figure 8: Comparaison LM-MLEM vs Line cone reconstruction

(a)

(b)

(c)
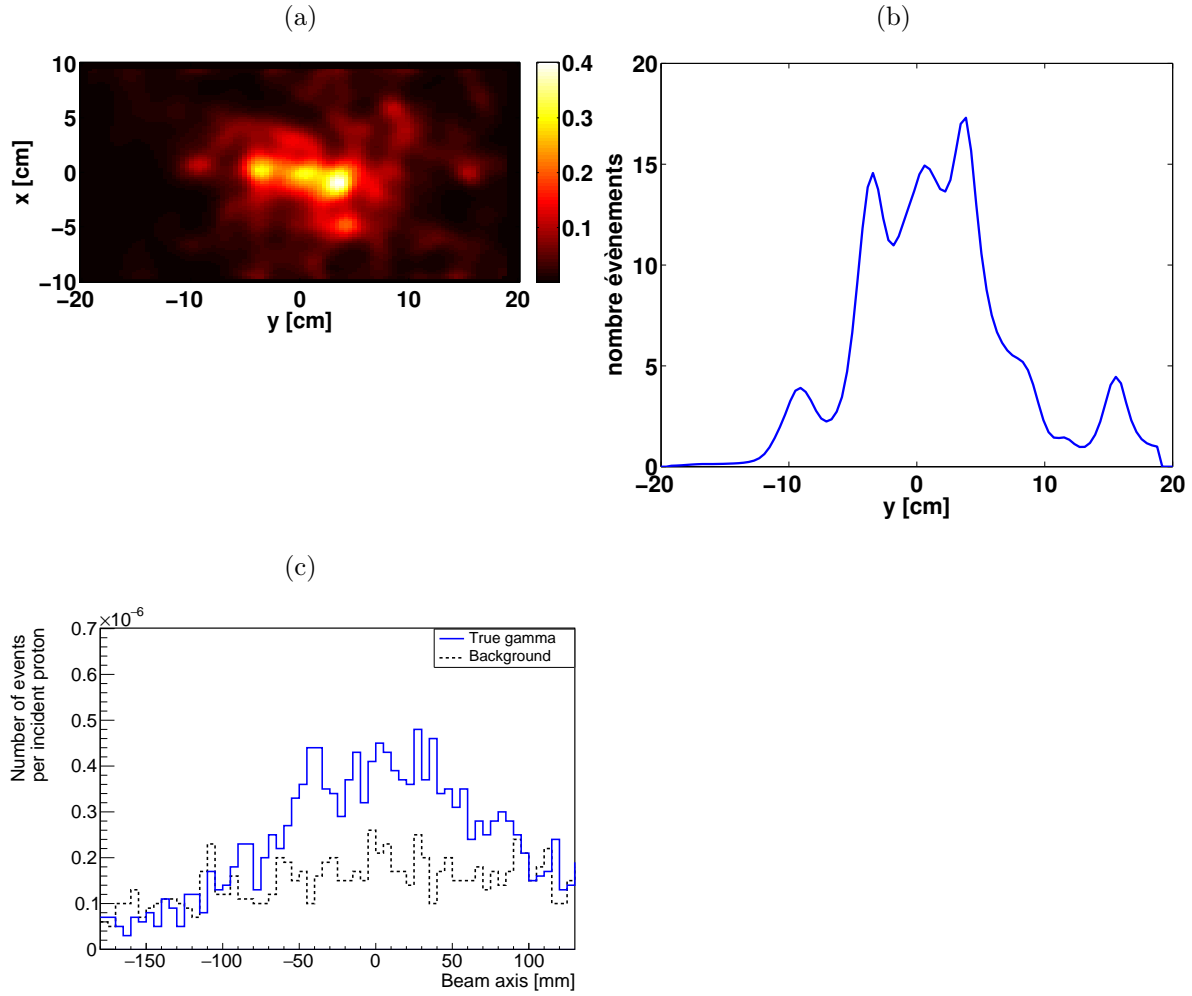
3.3. Comparaison LM-MLEM vs Line cone reconstruction

3.4. Compton camera precision

The informations given by a control device as the Compton camera have to be viable and as precise as possible. In order to estimate the precision of the Compton camera, a method is used.

Figure 9: Precision function of the incident protons .
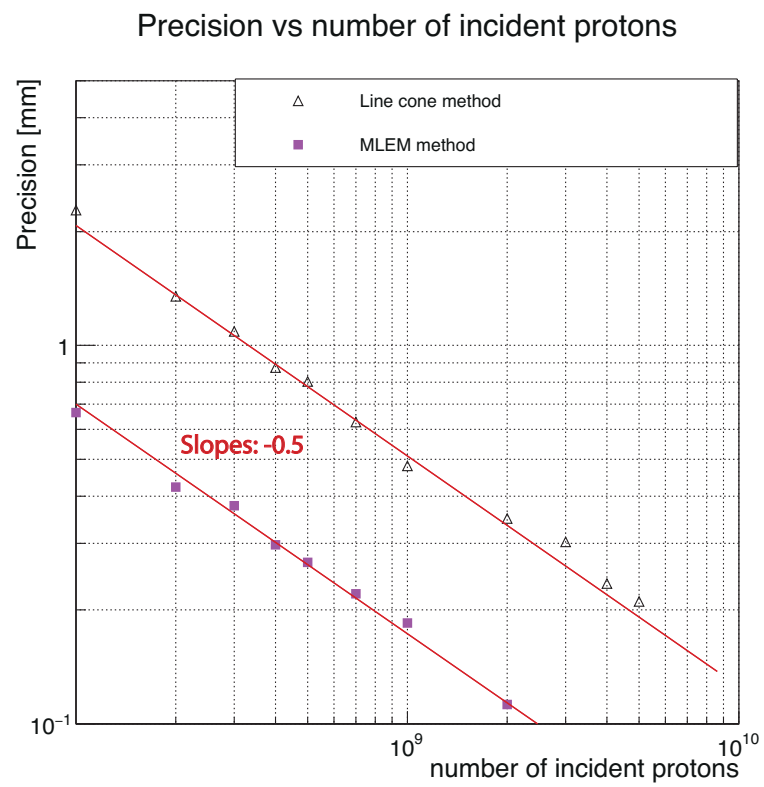
4. Discussion

Acknowledgments

[Cirrone et al., 2011] Cirrone, G. P., Cuttone, G., Mazzaglia, S. E., Romano, F., Sardina, D., Agodi, C., Attili, A., Blancato, A. A., De Napoli, M., Di Rosa, F., and others (2011). Hadrontherapy: a Geant4-based tool for proton/ion-therapy studies. *Prog. Nucl. Sci. Technol*, 2:207–212.

[Dedes et al., 2014] Dedes, G., Pinto, M., Dauvergne, D., Freud, N., Krimmer, J., LÃŇtang, J. M., Ray, C., and Testa, E. (2014). Assessment and improvements of Geant4 hadronic models in the context of prompt-gamma hadrontherapy monitoring. *Physics in Medicine and Biology*, 59(7):1747–1772.

[F Roellinghoff, 2014] F Roellinghoff, A. B. (2014). Real-time proton beam range monitoring by means of prompt-gamma detection with a collimated camera. *Physics in medicine and biology*, 59(5):1327–38.

[Toshito et al., 2010] Toshito, T., Bagulya, A., Lechner, A., Ivanchenko, V., Maire, M., Akagi, T., and Yamashita, T. (2010). New Geant4 electromagnetic physics developments for ion therapy applications. In *this conference*.